HHS Public Access

Author manuscript

Curr Biol. Author manuscript; available in PMC 2019 April 30.

Published in final edited form as:

Curr Biol. 2018 April 23; 28(8): 1179–1188.e3. doi:10.1016/j.cub.2018.02.061.

Hippocampal neural circuits respond to optogenetic pacing of theta frequencies by generating accelerated oscillation frequencies

Ipshita Zutshi[1,4], **Mark P. Brandon**[1,2,4,*], **Maylin L. Fu**[1], **Macayla Donegan**[1], **Jill K. Leutgeb**[1], and **Stefan Leutgeb**[1,3,5,*]

[1]Neurobiology Section and Center for Neural Circuits and Behavior, Division of Biological Sciences, University of California, 9500 Gilman Dr., San Diego, La Jolla, CA 92093, USA

[2]Department of Psychiatry, Douglas Hospital Research Centre, McGill University, 6875 LaSalle Blvd., Montreal, Quebec, Canada, H4H 1R3

[3]Kavli Institute for Brain and Mind, University of California, San Diego, 9500 Gilman Dr., La Jolla, CA 92093

[4]These authors contributed equally to this study.

[5]Lead contact

SUMMARY

Biological oscillations can be controlled by a small population of rhythmic pacemaker cells, or in the brain, also emerge from complex cellular and circuit-level interactions. Whether and how these mechanisms are combined to give rise to oscillatory patterns that govern cognitive function is not well understood. For example, the activity of hippocampal networks is temporally coordinated by a 7–9 Hz local field potential (LFP) theta rhythm, yet many individual cells decouple from the LFP frequency to oscillate at frequencies ~1 Hz higher. To better understand the network interactions that produce these complex oscillatory patterns, we asked whether the relative frequency difference between LFP and individual cells is retained when the LFP frequency is perturbed experimentally. We found that rhythmic optogenetic stimulation of medial septal GABAergic neurons controlled the hippocampal LFP frequency outside of the endogenous theta range, even during behavioral states when endogenous mechanisms would otherwise have generated 7–9 Hz theta oscillations. While the LFP frequency matched the optogenetically induced stimulation frequency, the oscillation frequency of individual hippocampal cells remained broadly distributed, and in a subset of cells, including interneurons, was accelerated beyond the new base LFP frequency. The inputs from septal GABAergic neurons to the hippocampus therefore do not appear to directly control the cellular oscillation frequency but rather engage cellular and circuit mechanisms that accelerate the rhythmicity of individual cells. Theta

*Correspondence to: Mark Brandon (mark.brandon@mcgill.ca) and Stefan Leutgeb (sleutgeb@ucsd.edu).

Author Contributions

M.P.B., I.Z., J.K.L. and S.L. designed the experiments. I.Z., M.P.B., M.L.F. and M.D. conducted experiments. I.Z. and M.P.B. performed analysis. M.P.B., I.Z., J.K.L., and S.L. wrote the paper.

Declaration of Interests

The authors declare no competing interests.

oscillations are therefore an example of cortical oscillations that combine inputs from a subcortical pacemaker with local computations to generate complex oscillatory patterns that support cognitive functions.

INTRODUCTION

Neuronal oscillations can arise from rhythmic activity in a small group of pacemaker cells, which impose oscillatory activity onto a broader network [1–3]. Alternatively, oscillations can also arise from cellular and synaptically-driven resonance [4–6]. However, there is limited knowledge on how afferent signals from neuronal pacemakers are combined with local mechanisms to give rise to the diversity of single-neuron activity. Hippocampal theta oscillations are an ideal paradigm to study this interaction, not only because of their functional relevance to memory and navigation, but also because they consist of at least two oscillators at closely related frequencies [7–9]. The spiking rhythmicity of individual hippocampal place cells occurs at a frequency that is approximately 1 Hz faster than the ongoing LFP frequency, and thus spiking exhibits a systematic phase advance across theta cycles. Theories of phase precession have proposed various mechanisms on how the frequency difference between the field potential and cellular oscillations emerges. This includes models that utilize two oscillators to achieve interference [7, 10] and models that use a single base oscillator in combination with an increasing ramp potential [11–13]. Despite differences in implementation, all of these models assume that the baseline LFP theta frequency is determined by an external pacemaker. In contrast, one theory of theta generation and phase precession has questioned whether intracellular and extracellular oscillations truly arise from different sources and has raised the possibility that a precisely phase-shifted summation of the faster spiking oscillations can generate the slower local field potential in the theta range without an external source to generate a baseline theta frequency [14].

Although mechanisms that support theta generation without external pacemakers have been observed at the cellular level [15] and when only local hippocampal circuits are preserved [6], it has long been known that long-range projections from the medial septal area to the hippocampus and medial entorhinal cortex are necessary for the presence of high-amplitude theta oscillations in awake, behaving animals. Lesions or inactivation of the medial septal area (MSA) cause a near-complete reduction of the amplitude of hippocampal and entorhinal theta [16–21]. In further support of a pacemaker within the septal area, subsets of MSA neurons exhibit rhythmic bursting that is phase locked to hippocampal theta oscillations [2, 22, 23]. Juxtacellular recordings from anatomically identified MSA cells suggest that these cells correspond to parvalbumin (PV)-expressing neurons in the medial septum [24]. These septal PV neurons are known to give rise to GABAergic long-range projections that terminate onto hippocampal and entorhinal GABAergic neurons, thus forming a disinhibitory circuit that is well positioned to mediate rhythmic disinhibition in hippocampal principal neurons [25–27].

Persistent theta oscillations are most prominent during locomotion [28], but can also be artificially elicited in anesthetized, immobile or slow-moving mice by rhythmic optogenetic

stimulation of the MSA PV neurons or fibers [29, 30]. Similarly, rhythmic hippocampal oscillations can also be driven by electrical stimulation of the fornix while the MSA is inactivated [31, 32] or by nonselective optical stimulation of septal cells [33, 34]. Taken together, these recordings have therefore shown that MSA stimulation can elicit theta-like oscillations in brain states when the theta rhythm is not typically observed. However, if the MSA were the pacemaker for theta oscillations, it would be expected that stimulation does not only artificially add an oscillatory signal, but also supersedes the ongoing oscillation. To test this hypothesis, we optogenetically stimulated MSA PV cells while mice were running on a track and while recording hippocampal LFP. In addition, we simultaneously recorded from place cells to examine the effects of optogenetic control of the MSA pacemaker on the oscillation frequency and phase coupling of individual cells. By performing the combined LFP and place cell recordings, we tested whether hippocampal circuits are prewired to generate an upward shift in the cellular oscillation frequency or whether cellular and LFP oscillation frequencies are controlled by separate circuit mechanisms.

RESULTS

Optogenetic stimulation of medial septal PV neurons was sufficient to supersede endogenous theta oscillations

Optogenetic stimulation of PV neurons in the MSA has been shown to control the hippocampal local field potential (LFP) frequency in anesthetized and immobile/slow-moving animals [29, 30]. We began by testing whether using a similar strategy during behavioral states when animals normally generate high-amplitude theta oscillations is adequate for not only driving hippocampal LFP, but also for superseding theta oscillations that are endogenously generated during movement. Channelrhodopsin (ChR2, 10 mice; oChIEF, 5 mice) was selectively expressed in MSA PV cells using an adeno-associated vector (AAV- Ef1α-DIO-hChR2-eYFP or AAV- Ef1α-DIO-oChIEF-mCitrine) in parvalbumin-cre (PV-cre) transgenic mice (Fig. 1a, Supplemental fig. 1a). An optic fiber (200 micron core diameter, 0.48 NA) was positioned just dorsal to the MSA for blue light laser stimulation (473 nm) at a total power of ~1–2 mW (32–63.6 mW/mm^2) at the tip of the fiber. In addition, a microdrive was implanted so that recording tetrodes could be advanced into the CA1 cell layer to chronically monitor local field potentials and the spiking of hippocampal pyramidal neurons (Supplemental fig. 1b). Animals were trained to run 10–14 laps counterclockwise on a large rectangular linear track (1.5 × 0.5 meters) for sugar pellets provided at one corner (Supplemental fig. 2a). While mice were running, rhythmic blue light stimulation (50 % duty cycle) was delivered to the MSA. For analysis of LFP data, we also used periods of stimulation in the home cage.

Septal control of theta oscillations depended on the extent of opsin expression

We performed rhythmic optogenetic stimulation of PV neurons in the MSA at 10 Hz (at the border of the endogenous theta frequency range) and at 12 Hz (beyond the endogenous range) to test whether we could precisely control the frequency of hippocampal field potentials while mice were running on the track. Onset of stimulation immediately caused a change in the frequency of hippocampal LFP oscillations that matched the stimulation frequency and superseded endogenously generated theta oscillations. Moreover, endogenous

theta oscillations promptly returned upon cessation of blue light stimulation (Figs. 1b, c, Supplemental fig. 1c). Green and amber light stimulation were used as controls and had substantially less effect on theta oscillations (Supplemental fig. 1d), consistent with weaker activation of channelrhodopsin at these wavelengths [35]. In addition, we did not observe detectable pacing of theta oscillations in mice in which the expression level of the viral vectors in the septum appeared weak or absent (Fig. 1d).

To quantify the relation between channelrhodopsin expression and pacing efficiency, we measured the volume of viral expression in the MSA and defined a metric for optogenetic control over theta. For the metric, we computed a wavelet-based amplitude ratio between the power within the endogenous range (7–9 Hz) and the power at the stimulation frequency (9–11 Hz for 10 Hz stimulation; 11–13 Hz for 12 Hz stimulation) (Supplemental fig. 1e and Online Methods, *Quantification of theta pacing*). As designed, the amplitude ratio clearly differentiated between stimulation and non-stimulation periods (Fig. 1e, Supplemental fig. 1f). Beyond a minimum threshold for opsin expression, we found a striking linear relation between MSA volume with opsin expression and pacing efficiency (Pearson correlation, n = 10, R = 0.93, $p = 0.0001$) (Fig. 1d). We also found no relationship between either the antero-posterior or dorso-ventral position of the optic fiber and pacing efficiency (Pearson correlation, antero-posterior: n = 10, R = 0.33, $p = 0.36$; dorso-ventral: n = 10, R = 0.069, $p = 0.85$) (Supplemental figs. 1g, h). All animals that were included in subsequent analysis showed opsin expression levels in the MSA that resulted in a minimum pacing efficiency (increase in amplitude ratio of at least 0.3 compared to no stimulation).

Theta frequency was controlled by septal stimulation while theta amplitude remained modulated by running speed

Even in animals with substantial control of LFP oscillations, we noted variability in the amplitude of paced oscillations. Because pacing of PV cells during urethane anesthesia has been reported to lead to more consistent amplitudes [29], we reasoned that the variability in the awake animal may be due to the running speed of the animal. With the high-temporal resolution of wavelet analysis, it is feasible to analyze the frequency and power as a function of the instantaneous running speed (computed from position sampled at 30 Hz). The wavelet analysis revealed that the LFP frequency was locked to the stimulation frequency at all running speeds, but that power increased with running speed to the same extent as in no-stimulation controls (ANCOVA, 10 Hz: n = 42 sessions, $F(1,1674) = 3.5$, $p = 0.06$; 12 Hz: n = 39 sessions, $F(1,1551) = 2.62$, $p = 0.1055$) (Figs. 2a–c). The amplitude of theta oscillations thus remained subject to endogenous modulation by the running speed of the animal, while external optogenetic modulation of MSA PV-expressing neurons efficiently set the frequency of theta oscillations. These results are consistent with models of theta generation in which the septum dictates theta frequency while cortical and/or cholinergic inputs determine the amplitude of theta oscillations [9, 19, 36].

Because stimulation of GABAergic septal terminals in hippocampus has previously been reported to decrease running speed [30], we next tested effects of our optical septal stimulation on movement. We observed an apparent increase in movement speed at the onset of light stimulation on the track, but control analysis revealed that the increase incidentally

emerged from the condition that the animal is required to move across a boundary to initiate the light stimulation at the beginning of the lap (Supplemental figs. 2a, b). To further confirm that light onset, when not conditional on animal movement, does not result in altered running speed, we performed recordings in the home cage where light stimulation was turned on and off at regular intervals irrespective of the animal's behavior (Supplemental fig. 2c). Under these conditions, theta frequency was effectively controlled by the stimulation but effects on movement speed were not observed (Supplemental figs. 2d, e). We also addressed whether the efficiency of pacing is dependent on the running speed, and found that at 10 Hz, pacing by MSA stimulation was particularly effective at rest and low running speeds, consistent with previous reports that theta can be paced optogenetically in this state [30, 34] (Supplemental fig. 2f). However, at 12 Hz in the home cage and at both stimulation frequencies on the track, the pacing efficiency was found to be similar across all running speeds (Supplemental fig. 2g).

Place coding by individual hippocampal cells remained intact during optogenetic pacing of hippocampal theta oscillations

After confirming that septal stimulation resulted in pacing of theta-like oscillations, we examined the effect of pacing on the spiking activity of CA1 pyramidal cells. We optogenetically stimulated the medial septum on alternate laps to compare the same cells in light-off versus light-on trials. This design allowed for spatial firing patterns, oscillatory patterns, and phase precession of the same set of neurons to be examined with and without stimulation. A lap-by-lap analysis of spatial maps showed a substantial but reversible spatial reorganization between stimulation and no-stimulation laps (Repeated measures one way ANOVA, rate map stability, 10 Hz: n = 150 cells, $F(1.9, 288.9) = 121.7$, $p < 0.0001$; 12 Hz: n = 116 cells, $F(1.9, 221.8) = 105.7$, $p < 0.0001$) (Figs. 3a–d, Supplemental fig. 3a, b). To determine whether this reorganization was a result of altered theta oscillations or a consequence of blue light shining into the animal's eyes during periods of optogenetic stimulation, we repeated the same paradigm in mice (n = 3) injected with a virus expressing cre-dependent GFP in the MSA. Recordings of CA1 cells in these control mice revealed that hippocampal neurons remapped to the same extent as in opsin injected mice, while there were no optically-mediated changes in their hippocampal LFP patterns (Supplemental figs. 3c–f). Therefore, differences in place fields between light-off and light-on trials arose due to sensory-mediated remapping. As expected for remapping, field locations differed but the spatial properties of the set of active cells in each condition (light-on vs. light-off) remained otherwise largely unchanged. Compared to laps with no light stimulation, hippocampal neurons in opsin expressing mice retained similar spatial coding properties and firing rates during stimulation at 10 Hz and 12 Hz, although there were minor differences of mean rate at 12 Hz and of peak rates and the number of fields per cell at both stimulation frequencies (Wilcoxon matched pairs signed rank test, 10 Hz: n = 150 cells, mean firing rate, $p = 0.095$; peak firing rate, $p = 0.004$; number of fields, $p = 0.009$; spatial information, $p = 0.91$; 12 Hz: n = 116 cells, mean firing rate, $p = 0.02$; peak firing rate, $p = 0.003$; number of fields, $p = 0.0001$; spatial information. $p = 0.70$) (Fig. 3e). Note that the preserved firing rates at 10 Hz and the minor decrease at 12 Hz imply that the average number of spikes per cycle decreased during optically driven compared to endogenous theta. In addition, place fields tiled the entire track for both baseline and stimulation laps (Fig. 3f, Supplemental figs. 3g,

h). Thus, the preservation of spatial coding allowed us to examine the precise timing of place cell firing without the need to correct for potential confounds from differences in place field size. However, in order to account for the spatial reorganization, place field boundaries were identified independently for light-on and light-off conditions.

The frequency of spiking rhythmicity partially scaled with optogenetically induced theta oscillations

We next analyzed the relation between place cell spiking and the optogenetically controlled hippocampal LFP. First, we did not find any difference in the spiking phase preference or mean resultant length of the cells' spiking between endogenous or optically paced theta oscillations for 10 Hz stimulation and only a minor increase in the mean resultant length for 12 Hz stimulation (10 Hz: n = 210 cells, mean phase, no stimulation, 209.2 ± 8.3 degrees, stimulation 201.8 ± 8.3 degrees, Wilcoxon matched-pairs signed rank test, $p = 0.60$; mean resultant length, no stimulation, 0.11 ± 0.006, stimulation, 0.12 ± 0.005, Wilcoxon matched-pairs signed rank test, $p = 0.36$; 12 Hz: n = 165 cells, mean phase, no stimulation, 216.8 ± 8.7 degrees, stimulation, 225.1 ± 8.50 degrees, Wilcoxon matched-pairs signed rank test, $p = 0.999$; mean resultant length, no stimulation, 0.11 ± 0.007, stimulation, 0.13 ± 0.008, Wilcoxon matched-pairs signed rank test, $p = 0.013$) (Supplemental fig. 4a).To then examine whether septal PV stimulation exhibited control of the rhythmic frequency of place cells, we calculated the spike-time autocorrelation for each neuron and used a fast-Fourier transform to obtain the predominant frequency (Fig. 4a). As previously reported for controls [7], the modulation frequency of the majority of principal cells (~65 %) was accelerated with respect to the endogenous LFP frequency during light-off laps. With light stimulation, there was an increase in the proportion of cells oscillating within 1 Hz above the optogenetically paced LFP frequency (10–11 Hz band for 10 Hz stimulation: 30 % during stimulation versus 16 % during no stimulation; 12–13 Hz band for 12 Hz stimulation: 25 % during stimulation versus 11 % during no stimulation) (Figs. 4b, c, Supplemental figs. 4b, c**)**. These shifts in the frequency of a subset of the principal cells while their overall distribution remained broad were in contrast to a more consistent shift in the frequency of interneurons to oscillation bands slightly above the stimulation frequency (10 Hz: from 0 % to 83.3 % in the 10–11 Hz band; 12 Hz: from 0 % to 78.3 % in the 12–13 Hz band) (Figs. 4d, e, Supplemental figs. 4d, e). We thus found that the acceleration was more consistent for interneurons in the pyramidal cell layer than for the population of pyramidal cells.

Importantly, these results also demonstrate that the cumulative proportion of principal cells that were spiking at frequencies above the predominant LFP frequency was lower during optogenetic stimulation compared to no stimulation (10 Hz: 56 % during stimulation versus 66 % during no stimulation; 12 Hz: 32 % during stimulation versus 63 % during no stimulation) (Supplemental fig. 4c), which would predict that phase precession with reference to optically driven oscillations is reduced. We therefore next examined whether hippocampal neurons retained phase precession in conditions with accelerated LFP frequency. We found that the average slope of phase precession was negative during no stimulation laps, but that phase precession was on average not retained during rhythmic optical stimulation at either 10 Hz (fields with significant slopes: no-stimulation laps, n = 54/207, stimulation laps, 36/175; mean ± SEM of all slopes: no-stimulation laps, −0.19

± 0.07, one-sample t test against slope of zero, t(188) = 2.84, $p = 0.005$, stimulation laps, −0.08 ± 0.09, one-sample t test, t(148) = 0.93, $p = 0.35$) or 12 Hz (fields with significant slopes: no-stimulation laps, n = 48/174, stimulation laps, 29/133; mean ± SEM of all slopes: no-stimulation laps, −0.18 ± 0.08, one-sample t test, t(153) = 2.25, $p = 0.026$, stimulation laps, 0.01 ± 0.10, one-sample t test, t(115) = 0.078, $p = 0.94$) (4f–h). Because cells no longer showed a consistent relation to LFP during 10 Hz and 12 Hz stimulation, it can be expected that the temporal organization among the cells in the population is substantially disrupted.

DISCUSSION

We investigated how hippocampal circuits responded to the pacing of theta oscillations by rhythmic optogenetic stimulation of MSA PV neurons. We found that stimulation controlled the frequency of hippocampal theta throughout the entire range of running speeds in freely moving mice. The finding that septal pacing of only PV neurons could supersede the endogenous theta oscillator is the most definite evidence so far for the hypothesis that these neurons function as a pacemaker for theta oscillations in the hippocampus. Interestingly, we also found a dissociation between the control of theta frequency and theta amplitude. The amplitude of the oscillations remained modulated by running speed [37] while the frequency was optogenetically controlled. Most strikingly, analysis of the firing patterns of hippocampal CA1 cells revealed complex interactions between the neuronal pacemaker for theta oscillations and local hippocampal computations. Rather than phase locking to the septal stimulation, a subset of hippocampal principal cells and most interneurons in the pyramidal cell layer responded with accelerated oscillation frequencies compared to the optogenetically imposed oscillation frequency. Taken together, our findings show that the MSA PV cells set the base frequency for LFP theta oscillations while local hippocampal mechanisms generate partially accelerated rhythmic spiking frequencies in response to oscillatory subcortical input to the network.

In agreement with previous studies, we confirmed that hippocampal theta oscillations could be controlled by stimulation of septal long-range projections to the hippocampus. However, previous studies showed these effects in anesthetized, head-fixed, or immobile/slowly moving mice [29, 30, 38, 39] or in rats only during immobility/slow movement [34] or while the endogenous septal oscillator was not active [31, 32]. The previous studies therefore showed that septal stimulation is sufficient for eliciting hippocampal LFP oscillations, but the conclusion that the septum is the pacemaker for endogenous theta oscillations requires that ongoing theta oscillations can be reliably occluded by septal stimulation. Here we show that it is possible with ChR2 and oChIEF expression in a high fraction of septal PV cells to fully pace oscillations at any running speed, which strongly suggests that we had control over a key element of the endogenous oscillator. In particular, the effectiveness of optogenetic pacing increased with increasing volume of medial septal opsin expression, which indicates that increasingly complete septal control over oscillations can supersede other endogenous oscillatory inputs to hippocampus, such as from the supramammillary nucleus. While we identified that control over frequency can be gained by stimulation of MSA PV cells, the relation between oscillation amplitude and the animal’s running speed was not altered. The dissociation between frequency and amplitude is consistent with the possibility that amplitude is not controlled by PV cells but rather by cholinergic mechanisms

or entorhinal inputs, or a combination thereof [19, 36, 40, 41]. Furthermore, the retained relation between oscillation amplitude and running speed, while we applied rhythmic optical stimulation during a wide range of speeds, also indicates that there were minimal indirect or circuit effects of our manipulations on neural mechanisms that control amplitude.

In addition to finding that septal PV neurons controlled hippocampal LFP frequency, we also found that the rhythmic stimulation generated an upward shift in the cellular oscillation frequency, and did so more effectively for interneurons than for principal cells. An elegant theoretical model by Geisler et al. [14] proposed that there is a direct coupling between the lower LFP frequency and the somewhat higher oscillation frequency of individual hippocampal cells. In their model, they considered that the next subpopulation of active hippocampal cells is activated with a delay, which adds to the cycle time of the cellular oscillator such that a secondary LFP oscillation with a longer cycle time and thus a lower frequency emerges. Although our findings are not consistent with the proposed dependence of the slower on the faster oscillator, we find effects in the reverse direction, with the slower frequency as the primary frequency, which then engages local mechanisms that generate a coupled, but accelerated secondary oscillation in interneurons and a small subset of principal cells. Furthermore, the retention of a broad range of frequency differences between the LFP and the remaining principal cells also shows that septal pacing does not simply result in the phase-locking of hippocampal principal cells, in contrast to what has been shown when local hippocampal PV cells or long-range GABAergic projections from entorhinal cortex are directly optogenetically stimulated [42, 43]. It can therefore be inferred that the preserved wide range of oscillation frequencies, along with the emergence of upward-shifted oscillations in only a subpopulation of cells while LFP oscillations are paced, is likely the result of the indirect targeting of principal cells by septal afferents through multiple local interneuron types in different hippocampal subregions (Supplemental fig. 4f) [23, 25, 27, 44].

The decoupling of cellular oscillators from a single pacing frequency raises the question about the nature of the local cellular or circuit mechanisms that give rise to the second oscillation frequency. One of the early models for phase precession [10–13] proposed that the accelerated frequency can emerge by combining a base inhibitory oscillation with a ramping excitation in excitatory cells. A prediction of the model is that it allows for oscillatory inhibition to generate an accelerated frequency for any cell that shows ramping excitation. Together with intracellular recording studies that show that intracellular membrane potentials ramp up as a cell’s place field is traversed [45], our results support that this class of models may apply to the small subpopulation of principal cells that was accelerated beyond the optical stimulation frequency. However, intracellular recordings did not only show excitatory ramps but also revealed membrane potential oscillations that were tightly phase-locked to the precise spike timing of the cells [45]. Because our optogenetic pacing frequency differed in most cases from the frequency of the cellular oscillations, the pacing could not have directly imposed oscillations that are synchronized with the spike timing of hippocampal principal cells. The observed dissociation between spike timing and the stimulation frequency thus suggests that intracellular oscillations are generated more indirectly than by direct coupling to the septal pacemaker. For example, once time differences in spiking compared to the base frequency have emerged in a subset of principal

cells, these oscillatory inputs could be propagated within the entorhino-hippocampal network through inhibitory interneurons, such that a combination of ramping inputs and oscillatory interference determines spike timing [45–47].

While many of the local circuit and cellular mechanisms for generating neuronal oscillations remain to be determined, our findings establish that two separate types of oscillations emerge within the hippocampus. Only the LFP frequency, which is thought to arise from synaptic currents [48], strongly depended on the pacemaker input from medial septal GABAergic cells. At the same time, the synaptic oscillations that were phase locked to the stimulation frequency did not result in a phase locking of interneurons within the CA1 cell layer, but rather in a consistent acceleration of these cells. The emergence of dual oscillations with a faster cellular than LFP frequency is consistent with the possibility that dendrite-targeting interneurons are paced by the subcortical inputs while interneurons within the cell layer continue to mediate feedback inhibition of principal cells and thus remain synchronized to the local cellular oscillations (Supplementary Fig. 4f). Taken together, our results therefore support both dual oscillator and ramping models of phase precession and that the complexity of the endogenous oscillation patterns may emerge from interactions between both mechanisms. Furthermore, we show that only the synaptic oscillations are directly controlled by the septal pacemaker, while more complex local oscillatory patterns in CA1 are only indirectly and partially controlled by these inputs. These results do not only advance our understanding of the emergence of complex biological oscillators, but also indicate that optogenetically controlling theta oscillations leaves many aspects of hippocampal circuit function intact. Such retained network behavior while artificially controlling a neural pacemaker has important implications for the potential use of brain stimulation therapies to treat memory disorders and suggests that improvements may in particular be achieved when returning the system to a state during which multiple oscillators can effectively interact. For example, theta oscillation frequency in animal models of Alzheimer's disease differs from controls [49], and our data suggest that artificial stimulation of the medial septum could restore an important aspect of the complexity of cortical oscillations in the theta frequency band.

STAR METHODS

Detailed methods are provided in the online version of this paper and include the following:

CONTACT FOR REAGENT AND RESOURCE SHARING

Further information and requests for resources and reagents should be directed to and will be fulfilled by the Lead Contact, Stefan Leutgeb (sleutgeb@ucsd.edu).

EXPERIMENTAL MODEL AND SUBJECT DETAILS

Eighteen male parvalbumin-cre transgenic mice (129p2-Pvalbtm1(cre)arbr/J, obtained from Jackson Laboratories), 2–6 month old, weighing 25–35 g, were subjects in this study (10 ChR2, 5 oChIEF, 3 GFP). Animals were housed individually in Plexiglas cages, maintained on a 12-h light/12-h dark cycle at ~90 % of the ad libitum weight, and given free access to water. All surgical and experimental procedures were approved by the Institutional Animal

Care and Use Committee at the University of California, San Diego and conducted according to NIH guidelines.

METHOD DETAILS

Surgery—Animals were implanted with a 16-channel microdrive aimed at the hippocampus and a fiber optic aimed at the medial septal area. Anesthesia was induced with a mixture of 3 % vaporized isoflurane in oxygen, and buprenorphine (0.02 mg/kg) was then administered for analgesia. Animals were continuously monitored for the level of anesthesia and were generally maintained at 1.5–2.0 % isoflurane for the duration of surgery. One anchor screw that was positioned just anterior and lateral to lambda was used as a recording ground. A Hamilton syringe or a glass pipette was used to deliver two 400 nl bolus injections of a cre-dependent viral vector (AAV1.EF1a.DIO.hChR2(H134R)-eYFP.WPRE.hGH, AAV_{DJ}.EF1a.DIO.oChIEF-mCitrine, or AAV_{DJ}.EF1a.DIO.eGFP) into the MSA (AP: +1.0 mm, ML: −0.7 mm, DV: −4.8 mm and −4.2 mm; angled 10 degrees medially). A custom assembled fiber optic was then lowered to a position just dorsal to the medial septum and secured in place to the anterior anchor screws (AP: +1.0 mm, ML: −0.7 mm, DV: −3.5 mm, angled 10 degrees medially). To implant the microdrive, a craniotomy was performed directly above the right hippocampus (AP: −1.9 mm, ML −1.8 mm), and the dura was removed. The microdrive was lowered to make contact with the dorsal surface of the brain and Neuroseal was applied to the remaining brain surface. The microdrive was then secured to the skull with a thick layer of dental acrylic. Tetrodes were lowered ~0.5 mm below the dorsal surface at surgery. Animals were sutured if necessary and were returned to their home cage for monitoring. Animals were allowed five days of recovery prior to behavioral testing.

Neurophysiology equipment and recordings—Single-unit and local field potentials were recorded using the chronically implanted microdrive, which contained four recording tetrodes (bundles of four 17 micron platinum-iridium (90/10%) wires). Tetrodes were gradually lowered to the CA1 pyramidal cell layers by rotating a thumb screw on the microdrive. A preamplifier (unity-gain operational amplifier located on the head stage) and tether connected the microdrive to a digital data acquisition system (Neuralynx, Inc.). A pulley-system was designed to counteract the weight of the tether and headstage. For single-units, recording tetrodes were targeted to the CA1 pyramidal layer. Signals were amplified (5,000–20,000 x) and bandpass filtered (600–6,000 Hz) to isolate spiking events. Spike waveforms above a trigger threshold (25–55 μV) were time-stamped and digitized at 32 kHz for 1 ms. LFP signals were band-pass filtered (0.1–9,000 Hz), sampled at 32,000 Hz, and amplified (5,000–20,000 x; Neuralynx, Bozeman, MT).

Experimental design—Recordings were conducted as animals ran 10–14 laps counterclockwise on a rectangle track. The rectangle track [150 × 50 cm with a track width of 10 cm] was constructed of black Plexiglas. Translucent guiderails (3 cm) were installed and a thin rubber sheet was applied to the track floor. The track was positioned in the center of a cue-rich room that contained a white light in one corner to serve as an orienting landmark. Following recovery from surgery, animals were trained daily on the track for a

minimum of one week prior to recordings while tetrode tips were gradually advanced to the CA1 pyramidal cell layer.

Position estimation—To track the position of the animal during each recording session, a ceiling-mounted video camera detected an array of light emitting diodes (LEDs) mounted on the recording head stage just above the head of the animal. The position of the LEDs was sampled at 30 Hz and the rat's x-y coordinate was calculated as the centroid of the LED array. Up to five consecutive missing samples, due to occlusion of the LEDs or reflections in the environment, were replaced by linear interpolation of position before and after the lost samples.

Optogenetic laser stimulation—A fiber optic patch cord was secured to the recording tether and connected to an OEM diode pumped steady state laser (DPSS, 473 nm wavelength). The DPSS laser was triggered with a TTL sent directly from a custom microprocessor controlled by Matlab through the Neuralynx NetCom development library. To control the output of the laser based on the animal's position on the track, position data collected by Cheetah was passed directly into the Matlab environment. The entire maze was divided into 116 3.5 cm-wide bins. A custom script determined whether the animal crossed a user-defined boundary on the track. Based on these calculations, the MATLAB script would then turn the laser on and off every alternate lap. Either 10 Hz or 12 Hz-stimulation was performed during each recording session. Laser stimulation was performed at a total power of ~1–2 mW (32–63.6 mW/mm^2) at the tip of the fiber. Light power above 2 mW did not further increase the efficacy of theta pacing.

Postmortem confirmation of recording locations—Tetrodes were not moved after the final recording session. Animals were overdosed with Sodium Pentobarbital and perfused intracardially with phosphate-buffered saline and then 4 % formaldehyde. Brains were extracted and stored in 4 % formaldehyde at 6 °C for at least 24 hours. Approximately 24 hours prior to slicing, brains were transferred into a 30 % sucrose solution for cryoprotection. A microtome was used to obtain coronal sections through the MSA and hippocampus. Hippocampal tissue was mounted on glass slides and stained with cresyl violet. Tetrodes that recorded well-isolated neurons were confirmed to have terminated in or near the principal cell layer of region CA1 (Supplementary fig. 1b). Medial septum tissue was mounted using VectaShield medium and imaged. Fluorescent microscopy confirmed that viral vector expression was robust and restricted to the MSA (the lateral septum does not contain PV-expressing neurons) and that the tips of fiber optics were just dorsal to or within the medial septum in animals with robust viral expression (Supplementary fig. 1a).

Quantification of viral vector expression and optic fiber placement—Sections containing the MSA of mice injected with a cre-dependent viral vector (AAV1.EF1a.DIO.hChR2(H134R)-eYFP.WPRE.hGH or AAV$_{DJ}$.EF1a.DIO.oChIEF-mCitrine) were imaged using a virtual slide microscope (Olympus, VS120) at 10x magnification using the same laser power and exposure time. Three sections (0.24 mm apart) along the antero-posterior extent of the MSA were chosen for each animal and subsequently analyzed using Fiji ImageJ. One region of interest (ROI) was drawn around the medial

septum, and two ROIs were drawn around the diagonal band of Broca in each hemisphere. The area of virus expression was calculated by subtracting the background from each image and calculating the area of opsin expression above a threshold of 0. The volume of opsin expression was then calculated by adding the area across the three sections per animal and multiplying by the distance between the sections. In addition, the depth of the optic fiber was determined from the section with the tip of the optic fiber cannula by calculating the distance from the top of the cortex to the tip of the optic fiber cannula.

Single unit identification—Methods for cluster cutting and cell tracking were the same as described previously [21]. Briefly, single-units were manually isolated offline using MClust, MATLAB 2009b (Redish, A.D. MClust. http://redishlab.neuroscience.umn.edu/MClust/MClust.html). Neurons were separated based on the peak amplitude, peak-to-valley amplitude, and energy of spike waveforms. Evaluation of the presence of biologically realistic inter-spike intervals, temporal autocorrelations, and cross correlations was used to confirm single-unit isolation. Neurons that were not separable in cluster space were removed from the analysis.

Amplitude ratio score—Local field potentials (LFPs) obtained from the hippocampus were referenced to ground. For each experiment, LFP from the tetrode with the highest mean power between 5–10 Hz was selected for analysis. A Morlet wavelet was used to compute the power across frequencies. LFP was downsampled to 500 Hz, and an amplitude ratio (Fig. 1, Supplementary fig. 1) was calculated, defined as the ratio of power within a ±1 Hz band of the stimulation frequency to power in the endogenous frequency band of 7–9 Hz. This permitted a sample-by-sample metric for determining the efficacy of optogenetic control of the LFP oscillation frequency.

Place field characterization—Position on the rectangular track was linearized into 116 3.5 cm-bins for analysis of spatial properties of hippocampal neurons. Rate maps were then computed as the number of spikes per time spent in each spatial bin and were smoothed by a pseudo-Gaussian kernel with a standard deviation of 1 bin. Spatial information was calculated as,

$$I = \sum_{i=1}^{N} p_i \frac{F_i}{F} \log_2 \frac{F_i}{F}$$

where I is the spatial information in bits/spike, p_i is the probability of occupancy in bin I, F_i is the mean firing rate for bin I, and F is the mean firing rate. Rate map stability was determined by calculating the correlation between rate maps for the 1st half of trials compared to the 2nd half of trials. Place fields were defined as cells that had a peak spatial firing rate greater than 5 Hz, and maintained >20 % of the peak rate for at least 20 cm and less than 140 cm. Cell were classified as principal cells if they had an average firing rate <5 Hz, and as interneurons if their average firing rate exceeded this threshold.

Single-cell temporal autocorrelations and frequency—For each cell, spike times were binned at a sampling rate of 500 Hz. The temporal autocorrelation between spike times

was calculated from the resulting vector. The power spectrum of the temporal autocorrelation was obtained via the Chronux function *mtspectrumumc()* using a padding factor equal to six powers of 2 over the sample size. The single-cell frequency was then taken as the frequency with maximum power in the 6–14 Hz range.

Theta phase detection and phase precession analysis—We used a waveform-based estimation of theta phase as described in ref. [50]. For each tetrode in the CA1 cell layer, the LFP signals were bandpass filtered between 1–60 Hz and used to find peaks, troughs, and zero crossings. Theta peaks were defined as 0 degrees, troughs as 180 degrees, and zero crossing as 90 and 270 degrees. We then interpolated phase values between these phase quadrants. Using these phase values, phase precession was then analyzed as described in detail in ref. [36]. Briefly, place fields were normalized between 0 and 1 from the beginning to end of the field. A circular-linear regression was then generated for spikes occurring within the bounds of the place field, and the slope of the regression line is reported. Data was analyzed separately for when laser stimulation was on or off, and analysis included within-session comparisons between 10 Hz-stimulation laps and no-stimulation laps or a comparison between 12 Hz-stimulation laps and no-stimulation laps. The data that are reported in the main text used boundaries of ±2.0 cycles to constrain the circular-linear regression, as in ref. [36]. We also repeated the analysis with the more conservative boundaries of ±1.1 and ±1.6 cycles and obtained matching results irrespective of the choice of parameter value (boundary of ±1.1, 10 Hz: fields with significant circular-linear regression: no stimulation laps, n = 44/207, stimulation laps, 22/175; mean ± SEM of all slopes: no stimulation laps, 0.10 ± 0.05, one-sample t test against slope of zero, $t(167) = 2.24$, $p = 0.026$, stimulation laps, −0.06 ± 0.05, one-sample t test, $t(129) = 1.41$, $p = 0.16$; boundary of ±1.1, 12 Hz: fields with significant circular regression values: no stimulation laps, n = 35/174, stimulation laps, 23/133; mean ± SEM of all slopes: no stimulation laps, 0.17 ± 0.05, one-sample t test, $t(142) = 3.62$, $p = 0.0004$, stimulation laps, −0.09 ± 0.06, one-sample t test, $t(102) = 1.61$, $p = 0.11$; boundary of ±1.6, 10 Hz: fields with significant circular-linear regression: no stimulation laps, n = 47/207, stimulation laps, 31/175; mean ± SEM of all slopes: no stimulation laps, −0.13 ± 0.06, one-sample t test against slope of zero, $t(176) = 2.29$, $p = 0.023$, stimulation laps, −0.08 ± 0.07, one-sample t test, $t(136) = 1.15$, $p = 0.25$; boundary of ±1.6, 12 Hz: fields with significant circular regression values: no stimulation laps, n = 42/174, stimulation laps, 27/133; mean ± SEM of all slopes: no stimulation laps, −0.17 ± 0.06, one-sample t test, $t(148) = 2.62$, $p = 0.009$, stimulation laps, 0.08 ± 0.07, one-sample t test, $t(105) = 1.055$, $p = 0.29$).

QUANTIFICATION AND STATISTICAL ANALYSIS

All statistical comparisons were calculated using MATLAB r2015b. Wilcoxon's paired, two-sided sign rank test (signrank, MATLAB) was used when comparing firing properties between no-stimulation and stimulation conditions. This test does not assume normality. An analysis of covariance (ANCOVA) test was performed to test for changes in speed modulation of theta power across running speed. Two-sided one-sample t-tests were used to compare phase precession slopes to the null hypothesis that the slope is equal to zero.

Supplementary Material

Refer to Web version on PubMed Central for supplementary material.

Acknowledgements

We thank Dr. B.K. Lim for providing viruses for the optogenetic experiments. We also thank C. Hyde, J. Davis, V. Yazdani, and G. DeGuia for technical assistance. This work was funded by NIH FMH096531A to M.P.B., Howard Hughes Medical Institute International Student Research Fellowship to I. Z., NIH R01 MH100349 to J.K.L., and Whitehall Foundation #2012-0685, NIH R21 MH100354, R01 NS086947, and R01 NS084324 to S.L.

REFERENCES

1. Saper CB (2013). The central circadian timing system. Curr Opin Neurobiol 23, 747–751. [PubMed: 23706187]
2. Petsche H, Stumpf C, and Gogolak G (1962). [The significance of the rabbit's septum as a relay station between the midbrain and the hippocampus. I. The control of hippocampus arousal activity by the septum cells.]. Electroencephalogr Clin Neurophysiol 14, 202–211. [PubMed: 14038334]
3. Kleinfeld D, Deschenes M, Wang F, and Moore JD (2014). More than a rhythm of life: breathing as a binder of orofacial sensation. Nat Neurosci 17, 647–651. [PubMed: 24762718]
4. Buzsaki G, and Draguhn A (2004). Neuronal oscillations in cortical networks. Science 304, 1926–1929. [PubMed: 15218136]
5. Atallah BV, and Scanziani M (2009). Instantaneous modulation of gamma oscillation frequency by balancing excitation with inhibition. Neuron 62, 566–577. [PubMed: 19477157]
6. Goutagny R, Jackson J, and Williams S (2009). Self-generated theta oscillations in the hippocampus. Nat Neurosci 12, 1491–1493. [PubMed: 19881503]
7. O'Keefe J, and Recce ML (1993). Phase relationship between hippocampal place units and the EEG theta rhythm. Hippocampus 3, 317–330. [PubMed: 8353611]
8. Skaggs WE, McNaughton BL, Wilson MA, and Barnes CA (1996). Theta phase precession in hippocampal neuronal populations and the compression of temporal sequences. Hippocampus 6, 149–172. [PubMed: 8797016]
9. Buzsaki G (2002). Theta oscillations in the hippocampus. Neuron 33, 325–340. [PubMed: 11832222]
10. Magee JC (2001). Dendritic mechanisms of phase precession in hippocampal CA1 pyramidal neurons. J Neurophysiol 86, 528–532. [PubMed: 11431530]
11. Mehta MR (2001). Neuronal dynamics of predictive coding. Neuroscientist 7, 490–495. [PubMed: 11765126]
12. Harris KD, Henze DA, Hirase H, Leinekugel X, Dragoi G, Czurko A, and Buzsaki G (2002). Spike train dynamics predicts theta-related phase precession in hippocampal pyramidal cells. Nature 417, 738–741. [PubMed: 12066184]
13. Mehta MR, Lee AK, and Wilson MA (2002). Role of experience and oscillations in transforming a rate code into a temporal code. Nature 417, 741–746. [PubMed: 12066185]
14. Geisler C, Diba K, Pastalkova E, Mizuseki K, Royer S, and Buzsaki G (2010). Temporal delays among place cells determine the frequency of population theta oscillations in the hippocampus. Proc Natl Acad Sci U S A 107, 7957–7962. [PubMed: 20375279]
15. Alonso A, and Llinas RR (1989). Subthreshold Na+-dependent theta-like rhythmicity in stellate cells of entorhinal cortex layer II. Nature 342, 175–177. [PubMed: 2812013]
16. Wilson JD, Bullock JY, Sutherland DC, Main C, and O'Brien KP (1978). Antinuclear antibodies in patients receiving non-practolol beta-blockers. Br Med J 1, 14–16. [PubMed: 23197]
17. Mitchell SJ, Rawlins JN, Steward O, and Olton DS (1982). Medial septal area lesions disrupt theta rhythm and cholinergic staining in medial entorhinal cortex and produce impaired radial arm maze behavior in rats. J Neurosci 2, 292–302. [PubMed: 7062110]

18. Mizumori SJ, McNaughton BL, Barnes CA, and Fox KB (1989). Preserved spatial coding in hippocampal CA1 pyramidal cells during reversible suppression of CA3c output: evidence for pattern completion in hippocampus. J Neurosci 9, 3915–3928. [PubMed: 2585060]
19. Yoder RM, and Pang KC (2005). Involvement of GABAergic and cholinergic medial septal neurons in hippocampal theta rhythm. Hippocampus 15, 381–392. [PubMed: 15630696]
20. Koenig J, Linder AN, Leutgeb JK, and Leutgeb S (2011). The spatial periodicity of grid cells is not sustained during reduced theta oscillations. Science 332, 592–595. [PubMed: 21527713]
21. Brandon MP, Bogaard AR, Libby CP, Connerney MA, Gupta K, and Hasselmo ME (2011). Reduction of theta rhythm dissociates grid cell spatial periodicity from directional tuning. Science 332, 595–599. [PubMed: 21527714]
22. King C, Recce M, and O'Keefe J (1998). The rhythmicity of cells of the medial septum/diagonal band of Broca in the awake freely moving rat: relationships with behaviour and hippocampal theta. Eur J Neurosci 10, 464–477. [PubMed: 9749709]
23. Joshi A, Salib M, Viney TJ, Dupret D, and Somogyi P (2017). Behavior-Dependent Activity and Synaptic Organization of Septo-hippocampal GABAergic Neurons Selectively Targeting the Hippocampal CA3 Area. Neuron 96, 1342–1357 e1345. [PubMed: 29198757]
24. Borhegyi Z, Varga V, Szilagyi N, Fabo D, and Freund TF (2004). Phase segregation of medial septal GABAergic neurons during hippocampal theta activity. J Neurosci 24, 8470–8479. [PubMed: 15456820]
25. Freund TF, and Antal M (1988). GABA-containing neurons in the septum control inhibitory interneurons in the hippocampus. Nature 336, 170–173. [PubMed: 3185735]
26. Gonzalez-Sulser A, Parthier D, Candela A, McClure C, Pastoll H, Garden D, Surmeli G, and Nolan MF (2014). GABAergic projections from the medial septum selectively inhibit interneurons in the medial entorhinal cortex. J Neurosci 34, 16739–16743. [PubMed: 25505326]
27. Unal G, Joshi A, Viney TJ, Kis V, and Somogyi P (2015). Synaptic Targets of Medial Septal Projections in the Hippocampus and Extrahippocampal Cortices of the Mouse. J Neurosci 35, 15812–15826. [PubMed: 26631464]
28. Vanderwolf CH (1969). Hippocampal electrical activity and voluntary movement in the rat. Electroencephalogr Clin Neurophysiol 26, 407–418. [PubMed: 4183562]
29. Dannenberg H, Pabst M, Braganza O, Schoch S, Niediek J, Bayraktar M, Mormann F, and Beck H (2015). Synergy of direct and indirect cholinergic septo-hippocampal pathways coordinates firing in hippocampal networks. J Neurosci 35, 8394–8410. [PubMed: 26041909]
30. Bender F, Gorbati M, Cadavieco MC, Denisova N, Gao X, Holman C, Korotkova T, and Ponomarenko A (2015). Theta oscillations regulate the speed of locomotion via a hippocampus to lateral septum pathway. Nature communications 6, 8521.
31. McNaughton N, Ruan M, and Woodnorth MA (2006). Restoring theta-like rhythmicity in rats restores initial learning in the Morris water maze. Hippocampus 16, 1102–1110. [PubMed: 17068783]
32. Shirvalkar PR, Rapp PR, and Shapiro ML (2010). Bidirectional changes to hippocampal theta-gamma comodulation predict memory for recent spatial episodes. Proc Natl Acad Sci U S A 107, 7054–7059. [PubMed: 20351262]
33. Robinson J, Manseau F, Ducharme G, Amilhon B, Vigneault E, El Mestikawy S, and Williams S (2016). Optogenetic Activation of Septal Glutamatergic Neurons Drive Hippocampal Theta Rhythms. J Neurosci 36, 3016–3023. [PubMed: 26961955]
34. Blumberg BJ, Flynn SP, Barriere SJ, Mouchati PR, Scott RC, Holmes GL, and Barry JM (2016). Efficacy of nonselective optogenetic control of the medial septum over hippocampal oscillations: the influence of speed and implications for cognitive enhancement. Physiological reports 4.
35. Mattis J, Tye KM, Ferenczi EA, Ramakrishnan C, O'Shea DJ, Prakash R, Gunaydin LA, Hyun M, Fenno LE, Gradinaru V, et al. (2011). Principles for applying optogenetic tools derived from direct comparative analysis of microbial opsins. Nat Methods 9, 159–172. [PubMed: 22179551]
36. Schlesiger MI, Cannova CC, Boublil BL, Hales JB, Mankin EA, Brandon MP, Leutgeb JK, Leibold C, and Leutgeb S (2015). The medial entorhinal cortex is necessary for temporal organization of hippocampal neuronal activity. Nat Neurosci 18, 1123–1132. [PubMed: 26120964]

37. Rivas J, Gaztelu JM, and Garcia-Austt E (1996). Changes in hippocampal cell discharge patterns and theta rhythm spectral properties as a function of walking velocity in the guinea pig. Exp Brain Res 108, 113–118. [PubMed: 8721159]
38. Vandecasteele M, Varga V, Berenyi A, Papp E, Bartho P, Venance L, Freund TF, and Buzsaki G (2014). Optogenetic activation of septal cholinergic neurons suppresses sharp wave ripples and enhances theta oscillations in the hippocampus. Proc Natl Acad Sci U S A 111, 13535–13540. [PubMed: 25197052]
39. Fuhrmann F, Justus D, Sosulina L, Kaneko H, Beutel T, Friedrichs D, Schoch S, Schwarz MK, Fuhrmann M, and Remy S (2015). Locomotion, Theta Oscillations, and the Speed-Correlated Firing of Hippocampal Neurons Are Controlled by a Medial Septal Glutamatergic Circuit. Neuron 86, 1253–1264. [PubMed: 25982367]
40. Bragin A, Jando G, Nadasdy Z, Hetke J, Wise K, and Buzsaki G (1995). Gamma (40–100 Hz) oscillation in the hippocampus of the behaving rat. J Neurosci 15, 47–60. [PubMed: 7823151]
41. Lee MG, Chrobak JJ, Sik A, Wiley RG, and Buzsaki G (1994). Hippocampal theta activity following selective lesion of the septal cholinergic system. Neuroscience 62, 1033–1047. [PubMed: 7845584]
42. Royer S, Zemelman BV, Losonczy A, Kim J, Chance F, Magee JC, and Buzsaki G (2012). Control of timing, rate and bursts of hippocampal place cells by dendritic and somatic inhibition. Nat Neurosci 15, 769–775. [PubMed: 22446878]
43. Melzer S, Michael M, Caputi A, Eliava M, Fuchs EC, Whittington MA, and Monyer H (2012). Long-range-projecting GABAergic neurons modulate inhibition in hippocampus and entorhinal cortex. Science 335, 1506–1510. [PubMed: 22442486]
44. Frotscher M, and Leranth C (1985). Cholinergic innervation of the rat hippocampus as revealed by choline acetyltransferase immunocytochemistry: a combined light and electron microscopic study. J Comp Neurol 239, 237–246. [PubMed: 4044938]
45. Harvey CD, Collman F, Dombeck DA, and Tank DW (2009). Intracellular dynamics of hippocampal place cells during virtual navigation. Nature 461, 941–946. [PubMed: 19829374]
46. Leung LS (2011). A model of intracellular theta phase precession dependent on intrinsic subthreshold membrane currents. J Neurosci 31, 12282–12296. [PubMed: 21865471]
47. Jaramillo J, Schmidt R, and Kempter R (2014). Modeling inheritance of phase precession in the hippocampal formation. J Neurosci 34, 7715–7731. [PubMed: 24872575]
48. Einevoll GT, Kayser C, Logothetis NK, and Panzeri S (2013). Modelling and analysis of local field potentials for studying the function of cortical circuits. Nat Rev Neurosci 14, 770–785. [PubMed: 24135696]
49. Goutagny R, Gu N, Cavanagh C, Jackson J, Chabot JG, Quirion R, Krantic S, and Williams S (2013). Alterations in hippocampal network oscillations and theta-gamma coupling arise before Abeta overproduction in a mouse model of Alzheimer's disease. Eur J Neurosci 37, 1896–1902. [PubMed: 23773058]
50. Belluscio MA, Mizuseki K, Schmidt R, Kempter R, and Buzsaki G (2012). Cross-frequency phase-phase coupling between theta and gamma oscillations in the hippocampus. J Neurosci 32, 423–435. [PubMed: 22238079]

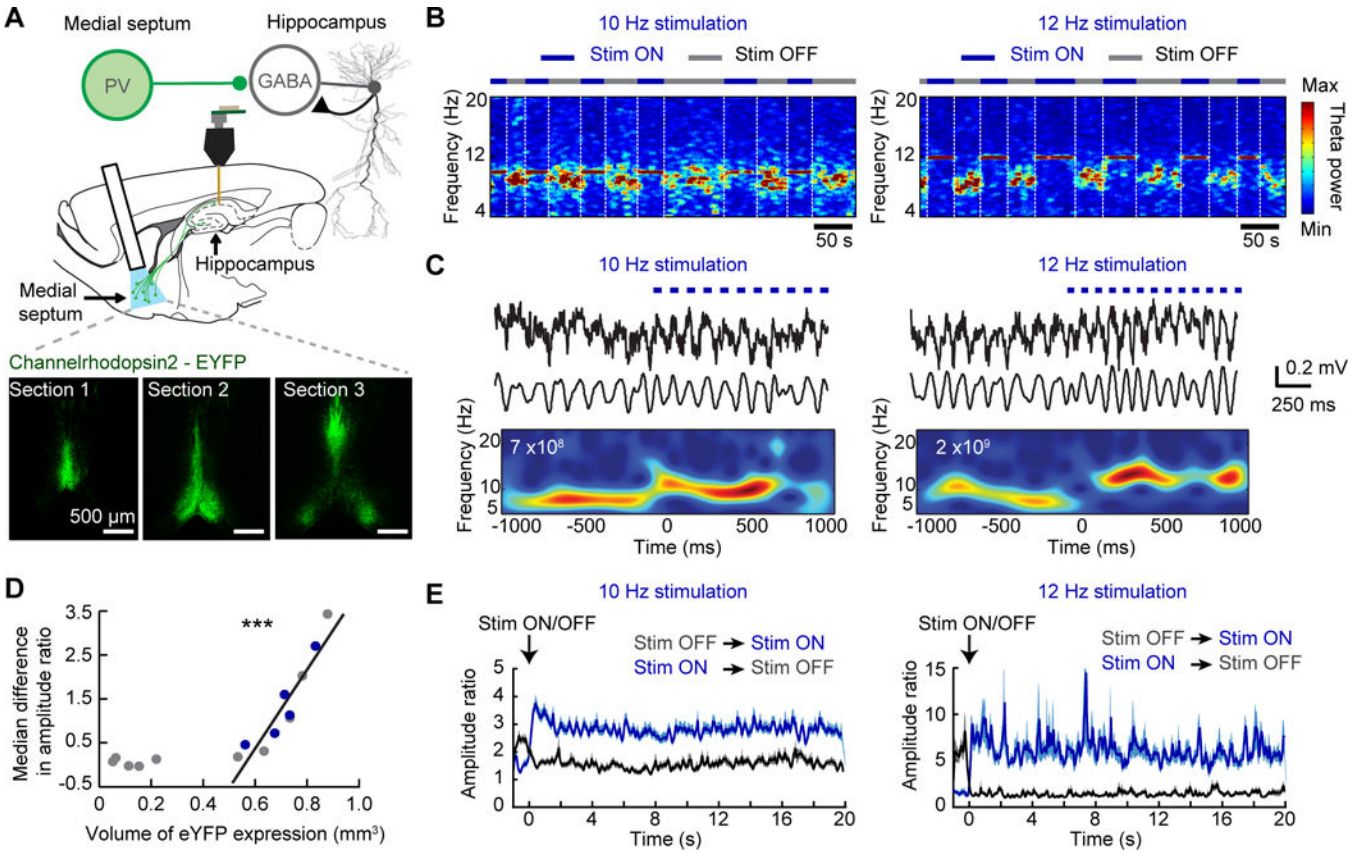

Figure 1. Rhythmic stimulation of medial septal PV neurons controls the frequency of theta oscillations in freely behaving mice.

(**A**) *Top,* Schematic of optogenetic and recording approach during behavior on the rectangle track. Cre-dependent channel rhodopsin (ChR2) or oChIEF was expressed by targeting an AAV to the medial septal area (MSA) of PV-cre transgenic mice. Opsin expressing PV neurons were optically stimulated while we performed recordings of CA1 cells and LFP. *Bottom*, Example images demonstrate how virus expression was quantified by determining the area of fluorescence in three sections along the antero-posterior axis of the MSA. (**B**) Example spectrograms of LFP from the CA1 region of the hippocampus as animals ran around a rectangular track. PV neurons in the MSA were optogenetically activated at either 10 Hz (*left*) or 12 Hz (*right*) on every alternate lap. *White stippled lines* mark the end of each lap. The LFP frequency was completely entrained to the stimulation frequency during light-on trials. (**C**) Example LFP traces are shown for one second before and one second after the onset of 10 Hz (*left*) or 12 Hz (*right*) optical stimulation of MSA PV neurons. *From top to bottom*, raw traces, bandpass filtered (5–25 Hz) traces, and a wavelet transform of the traces. Stimulation resulted in an increased LFP frequency within one theta cycle. *White text and red color* within the plot, maximum wavelet power. (**D**) Scatter plot of the volume of YFP expression in the MSA and the pacing efficiency across all animals. A linear relationship was found once the expression exceeded a minimum threshold (0.5 mm^3). The blue dots correspond to mice used for single unit analyses. (**E**) The average amplitude ratio of all data collected for 20 seconds after the onset of stimulation (ON laps, *blue traces*) and

for 20 seconds after stimulation was stopped (OFF laps, *black traces*) at 10 Hz (*left*) and 12 Hz (*right*). **** p<0.001.*

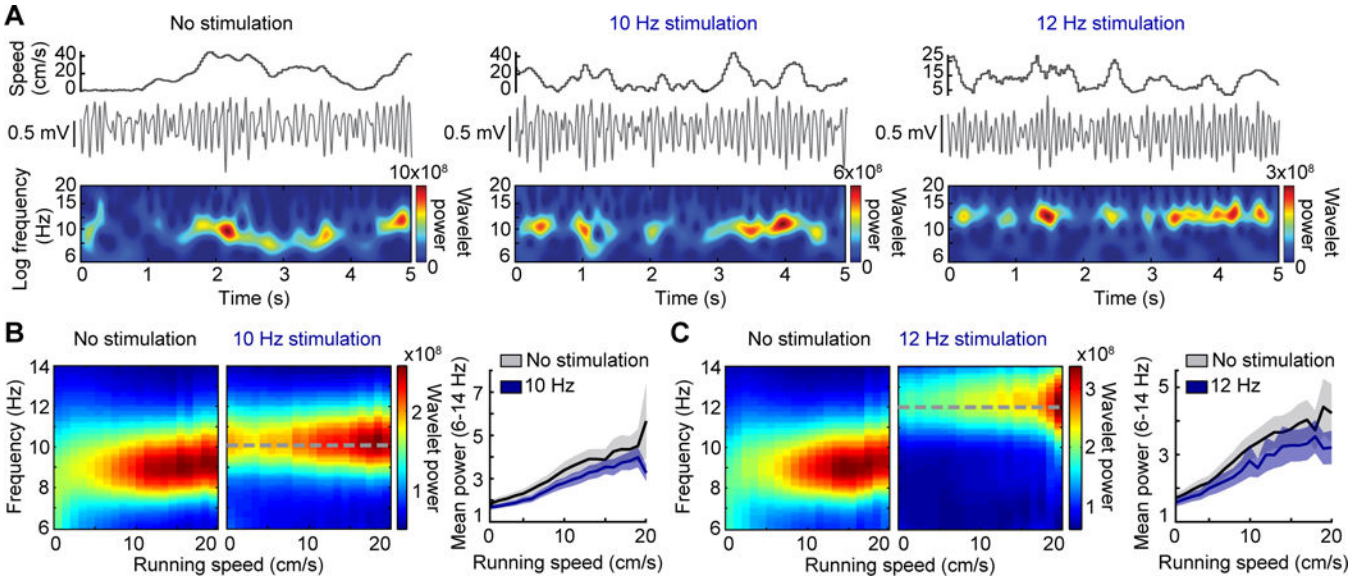

Figure 2. Theta amplitude increases with running speed during pacing.

(**A**) Hippocampal LFP and wavelet power is displayed as a function of running speed for periods without stimulation, 10 Hz stimulation, and 12 Hz stimulation of septal PV neurons. Note that the wavelet power was highest during periods with fast running speeds in both baseline and stimulation conditions. (**B, C**) (*Left*) Mean spectrograms over all recording sessions show the amplitude and frequency distribution across running speeds. (*Right*) Mean (± SEM) normalized power of theta oscillations (averaged over 6–14 Hz) is plotted by running speed. Stimulation controlled the frequency but did not preclude the modulation of theta amplitude by running speed during either 10 Hz or 12 Hz stimulation.

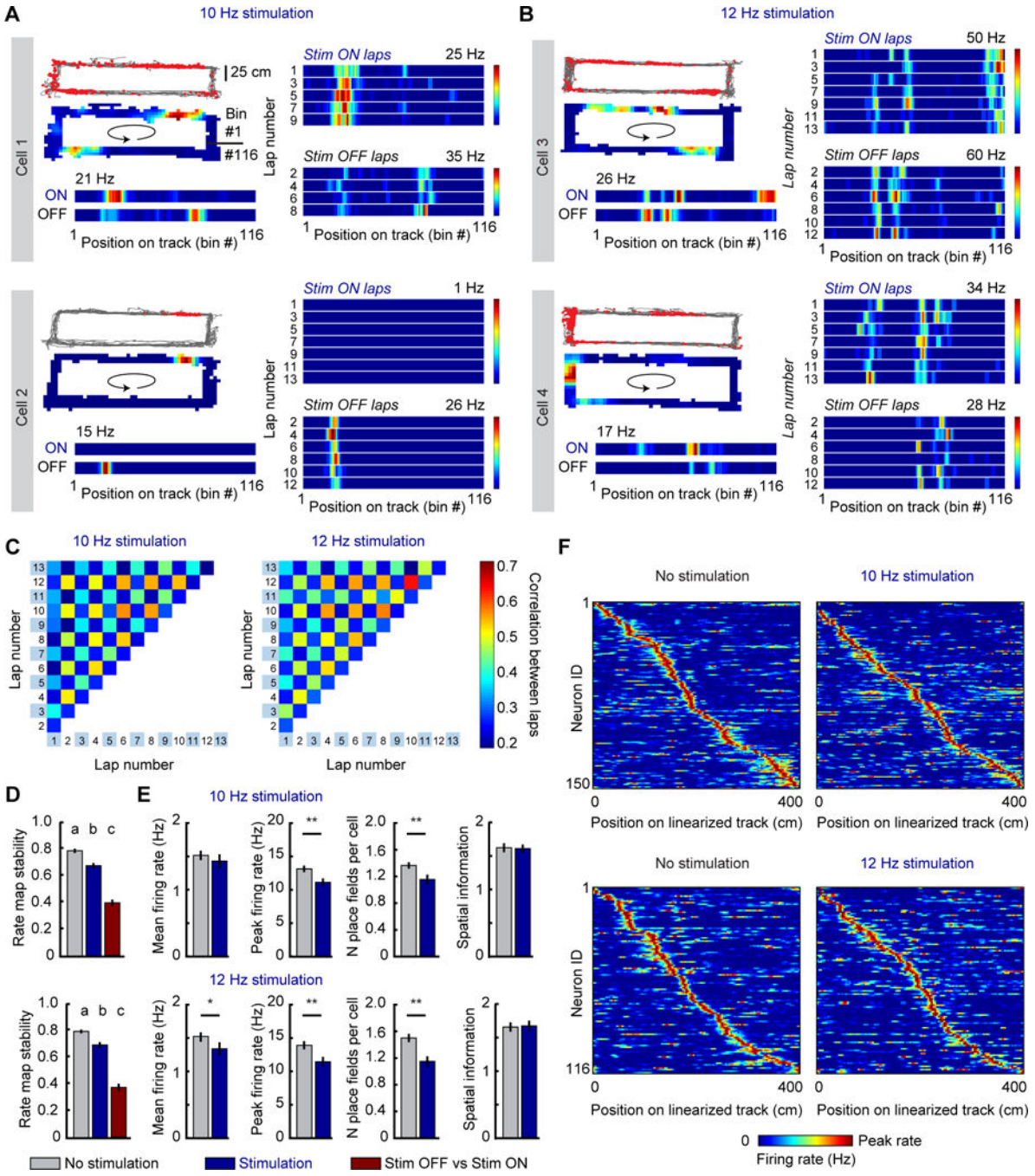

Figure 3. Spatial firing is preserved during optogenetic pacing of theta oscillations.

Example place fields on the track are shown for (**A**) 10 Hz and (**B**) 12 Hz stimulation sessions. *Left of each panel*, Path in grey with the cell's spikes overlaid as red dots, the same cell's rate map over the entire session (arrow shows the direction of running), and the cell's linearized rate map averaged independently for stimulation and no stimulation laps. The peak rate of the cell is indicated above the map. *Right of each panel,* Rate map of the same cell for individual stimulation ON and OFF laps. Lap number is to the left of each rate map. The spatial firing patterns of the cells reliably switch back and forth between the light-on

and light-off conditions. (**C**) A correlation matrix was computed to determine the stability of place cells across multiple laps in a session. Odd numbered laps are light ON, and even numbered laps are light OFF. The chessboard appearance of the matrix shows that rate maps were stable within light-on and light-off trials, but reorganized between the two. (**D**) Mean (± SEM) stability of rate maps. Within light-off and within light-on stability was higher than stability between conditions. Significantly different groups are assigned separate letters (a, b, c). (**E**) The firing properties of place cells (mean firing rate, peak firing rate, and number of place fields per cell) showed minor differences between no-stimulation and stimulation trials, but importantly, the spatial information of cells was not affected despite remapping during stimulation. Histograms depict mean ± SEM. (**F**) The positions of the fields along the linear track for all cells that were recorded during baseline and stimulation laps. Cells are ordered by their position on the track independently for the no-stimulation and the stimulation condition. Fields were distributed along the entire track in all conditions. * $p<0.05$, ** $p<0.01$.

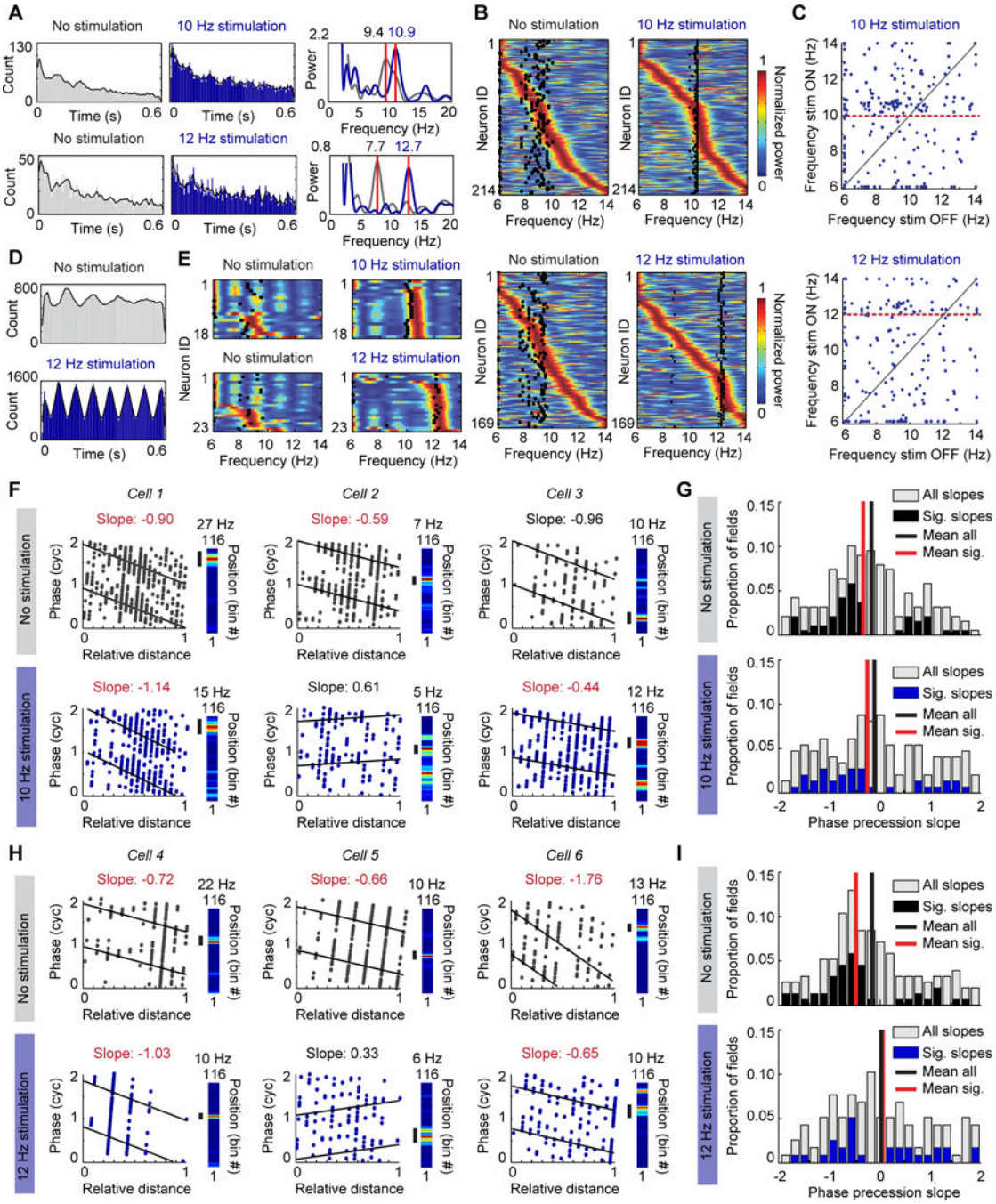

Figure 4. The oscillation frequency of hippocampal neurons is accelerated compared to the LFP frequency during optogenetic pacing of theta-like oscillations.

(A) *Left,* Spike time autocorrelation of two example cells (*grey*, no-stimulation laps; *blue*, stimulation laps). *Right,* Power calculated from the spike-time autocorrelation of the same cells shows an accelerated frequency compared to the stimulation frequency in the stimulation condition. Variability in spiking occasionally resulted in additional oscillation peaks below the theta range, but peaks within the theta range were consistently observed. (**B**) Color-coded power (*blue to red*) calculated from the autocorrelation function of

individual pyramidal cells during no-stimulation laps is compared to the mean LFP frequency (*black dots*). Most cells (i.e., those with peak power to the right of the black dots) were spiking rhythmically at frequencies higher than the LFP frequency during no stimulation laps. During stimulation, the oscillation frequency of a subset of principal cells was accelerated compared to the stimulation frequency. (**C**) The peak frequency of each cell (*blue dots*) during no-stimulation laps is plotted against its peak frequency during stimulation laps. The *red dotted line* highlights the stimulation frequency. (**D**) Same as A, but for an example interneuron recorded from the CA1 pyramidal cell layer. The rhythmicity of the interneuron was accelerated by the stimulation. (**E**) Same as B, but for interneurons. Most interneurons were strongly entrained to frequencies higher than the LFP frequency during 10 Hz and 12 Hz stimulation. (**F)** Phase precession slopes of three example cells during no-stimulation laps (*top)* and 10 Hz stimulation laps (*bottom*). Precession was calculated with reference to endogenous frequency during no-stimulation laps and with reference to the paced frequency during stimulation laps. For each cell, the linearized rate map on the track is provided to the *right* with the field used for calculating phase precession marked by a *black bar*. Cell 3 is an example of a field that remaps to a new location during stimulation, and where the new field reliably phase precesses. Significantly negative slopes are highlighted by noting the slope in *red font*. (**G**) *Top*, Histogram depicting the slopes of all fields during no-stimulation laps (*grey*), overlaid with only the significant slopes in *black*. *Bottom,* Histogram depicting the slopes of all fields during 10 Hz stimulation laps (*grey*), overlaid with only the significant slopes in *blue*. (**H**, **I**) Same as F and G but for cells recorded during 12 Hz stimulation sessions.